Low temperature magnetic properties of a $Ni_{50}Mn_{34}In_{16}$ ball-milled metamagnetic shape memory alloy

S. Larumbe[1,2], I. Unzueta[4,5],V. Sánchez-Alarcos[1,2], J.I. Pérez-Landazábal[1,2], V.Recarte[1,2], J.A.García[3,5] and F. Plazaola[4]

[1]Departamento Física. Universidad Pública de Navarra, Campus de Arrosadia, 31006 Pamplona, Spain

[2]Institute for Advanced Materials (INAMAT), Universidad Pública de Navarra, Campus de Arrosadía, 31006 Pamplona, Spain

[3]Fisika Aplikatua II Saila, Euskal Herriko Unibersitatea UPV/EHU, p.k. 644, 48080 Bilbao, Spain

[4]Elektritate eta Elektronika Saila, Euskal Herriko Unibersitatea UPV/EHU, p.k. 644, 48080 Bilbao, Spain

[5]BC Materials (Basque Centre for Materials, Applications and Nanostructures), 48080 Leioa, Spain

Abstract. The effect of the atomic disorder induced by ball-milling on the structure and the magnetic properties has been analyzed in a $Ni_{50}Mn_{34}In_{16}$ metamagnetic shape memory alloy. The as-milled samples displayed an amorphous structure which crystallizes to a disorder B2 structure on annealing. On further annealing, several recovery processes leading to the austenitic $L2_1$ structure and the subsequent martensitic transformation are observed. As a result of the recovery processes, the magnetic order drastically varies concurrent with the long-range atomic order. In particular, the magnetism evolves from a frustrated magnetic state compatible with a canonical spin-glass, observed in the amorphous structure, to the well-developed ferromagnetic state.

1. Introduction

Ferromagnetic shape memory alloys (FSMA) have been thoroughly studied due to their interesting and promising applications such as magnetic actuators or refrigerator systems related to different phenomena (superelasticity, memory effect, giant magnetoresistance (GMR) or the magnetocaloric effect)[1–4].FSMA are Heusler alloys that are based on intermetallic compounds basically defined by a X_2YZ stoichiometry where X is usually a transition metal, Y: Mn and Z an element from the IIIA, IVA or VA groups of the periodic table. Heusler alloys undergo a first order transition known as the martensitic transition that takes place between two structural phases, a low temperature phase (martensitic phase) with a low symmetry structure and a high temperature phase (austenitic phase) with a cubic structure. NiMnX, where X:In,Sn or Sb constituted the so-called metamagnetic FSMA, in which the structural transition can be induced by the application of a magnetic field since the magnetic field provokes a shift to lower temperatures of the structural transition [4,5].

The magnetic ordering in Ni-Mn-X Heusler alloys is associated to the indirect magnetic exchange between Mn-Mn[6], [7] and to the direct exchange between Mn-X. Their magnetic properties are therefore greatly influenced by the intrinsic composition and long-range atomic order. The composition has been commonly pointed out as a critical factor to analyze in the final magnetic properties of these alloys. This result can be deduced from the change of the valence electron concentration (e/a) and therefore on the different conduction electrons involved in the Ruderman-Kittel-Kasuya-Yosida (RKKY) indirect exchange [8]. In this respect, some works have outlined that the excess of Mn atoms with respect to the stoichiometric composition gives rise to an antiferromagnetic (AFM) exchange interaction [9]. On the other hand, the antiferro-ferromagnetic character of the Mn-Mn magnetic interactions is also affected by the variations on the interatomic

distances brought by atomic ordering. With respect to Ni-Mn-In alloys, the atomic order can be controlled by different thermal treatments (contrary to what occurs in Ni-Mn-Sn and Ni-Mn-Sb, where the $L2_1$ structure is extraordinary stable and no long-range order variation is achieved from thermal treatment [10]). In particular, higher quenching temperatures induce a higher retained disorder degree and therefore higher martensitic transformation temperatures and lower austenitic Curie temperatures [11], [12].

Structural disorder has arisen as a critical factor for the appearance of spin glass behavior in different magnetic oxides [13–16], nanosized particles [17] or metallic alloys [9,18,19]. Spin glasses are described as systems that merge structural and magnetic disorder, giving rise to a magnetic frustration and short-range order (competition between FM and AFM exchange interactions). A freezing temperature (T_f) is defined, below which the spins are randomly oriented. Generally, it can be distinguished between canonical and cluster spin glasses. Canonical spin glasses are characterized by the existence of randomly oriented isolated magnetic moments. On the other hand, the cluster spin glasses are composed of collective disordered spins in different regions of the material which are dispersed in the metallic matrix with RKKY indirect exchange interactions [19]. The difference between both types of spin glasses lies on the different interaction and dynamic behavior.

In recent years, several attempts have been carried out in order to determine the effect of defects on the characteristic structural transition and magnetic properties in different FSMA (Ni-Mn-Ga, Ni-Mn-In and Ni-Mn-Sn) prepared by different methods (ball milling or laser ablation) [20–24]. It has been already reported that the decrease of the size in Ni-Mn-Ga particles prepared by ball milling led to a distortion of the structure in such a way that it was necessary to anneal the sample at high temperatures (1073 K) to induce the crystallization up to a $L2_1$ phase in order to observe the expected martensitic transition. Nevertheless, low temperature annealing (<573 K) only allowed the crystallization

process to a disordered bcc structure [22]. For the case of the metamagnetic alloys, this effect has been scarcely analyzed in the bibliography. As in NiMnGa powders, the austenitic phase is obtained only after heating up to high temperatures in NiMnSn (1223 K) [25] and NiMnIn particles (673 K) [26]. In this latter case, a magnetic transition from paramagnetic-like to spin-glass state is suggested to occur at low temperatures as a consequence of the induced defects.

In this work, the influence of mechanical induced disorder on the magnetic properties of a $Ni_{50}Mn_{34}In_{16}$ metamagnetic shape memory alloy is analyzed. The as-milled samples displayed an amorphous structure and, on heating, several recovery processes are observed. In particular, the magnetism at low temperatures evolves from a frustrated magnetic state compatible with a canonical spin-glass, observed in the amorphous structure, to the well-developed ferromagnetic state after crystallization.

2. Experimental

A $Ni_{50}Mn_{34}In_{16}$ alloy was prepared by means of arc melting under argon atmosphere. The as-cast ingots was homogenized at 1073 K during 15h and then quenched into iced water. Afterwards, the alloy were subjected to a ball milling process in an argon atmosphere during different effective milling times (10h and 40h) at room temperature. In order to avoid oxidation, the samples were milled during 5 minutes (effective-milling time) and then stopped for 10 minutes to prevent overheating of the sample and grinding jars. Ball milling was performed at 300 rpm using a Retsch PM4 with a ball:powder ratio of 7:1 and 7 balls of 5 mm diameter. Both jars and balls were of tungsten carbide (WC). The structural transformations and the possible recovery processes taking place on treating the as-milled powder samples were characterized by Differential Scanning Calorimetry

(DSC) by means of a Q-100 DSC (TA Instruments) calorimeter with a heating rate of 10K/min under nitrogen atmosphere (flow of 50mL/min). Room temperature X-Ray Diffraction (XRD) patterns were measured with a Diffractometer model Siemens D5000 with a step of 0.02° in order to analyze the crystallographic structure of the as-milled sample. The final chemical composition was determined by Energy Dispersive Scattering (EDS) with a Jeol JSM-5610LV Scanning Electron Microscope (SEM). In both cases (samples milled for 10h and 40h) the composition was confirmed to be around the nominal composition $Ni_{50}Mn_{34}In_{16}$. Finally, the magnetic characterization was carried out in a SQUID magnetometer (QD MPMS XL7).

3. Results and discussion

Figure 1 shows the DSC thermograms measured for the as-milled samples along with that corresponding to the bulk material (see inset). Substantial differences are observed comparing both types of samples. The exothermic and endothermic peaks corresponding to the forward and reverse martensitic transformation, respectively, are observed below room temperature (at T_M^{for} and T_M^{rev}, respectively) in the bulk, together with a non-hysteretic λ-type shoulder around 300 K linked to the ferro↔para magnetic transition at the Curie temperature, T_C. In the powdered samples, in turn, no transformation is detected neither below nor around room temperature, and just three exothermic peaks are observed in both cases on heating above 350 K. In particular, one broad shoulder (S) around 400 K and two intense peaks (P1 and P2) between 500K and 600K. The first shoulder has been commonly related to a glass transition temperature in different amorphous metallic alloys, although in some ball milled systems is covered up by the exothermic peaks related to the crystallization process. The temperature associated to this first transition remains nearly

constant for both samples, whereas the P1 and P2 peaks shift to higher temperatures with the increasing milling time. In order to determine the structure of the as-milled alloys as well as to ascertain the possible structural processes linked to exothermic peaks observed in the thermograms, X-Ray diffraction measurements have been performed. Figure 2 shows the room temperature diffractograms obtained both on the as-milled samples (Figure 2a) and on the sample milled for 40 h and heated up to temperatures just above the P1 and P2 DSC peaks (Figures 2a and 2c, respectively). The as-milled samples show a broad peak that evidences the achievement of an amorphous phase as a result of the structural distortion caused by the ball milling process. Once the milled sample is heated up to above the P1 peak (536 K), some Bragg reflections appear in the diffractogram, indicating an initial crystallization stage to the cubic B2 structure. On further heating above the P2 peak (673 K), no other structural transformation takes place and just an increase of the intensity of the B2 diffraction peaks is observed. Therefore, the two exothermic peaks detected in the DSC curves could be related to a two-stage crystallization process from the amorphous state to a cubic B2 structure (as consequence of the low contrast of X-Ray scattering lengths of Ni, Mn and In, the degree of long-range atomic order could not be evaluated from the diffractograms). Subsequent DSC measurements performed in the thermal treated samples confirmed that such B2 structure does not undergo martensitic transformation, and that an annealing treatment above 1173K was needed to achieved the austentic $L2_1$ Heusler structure (futher microstructural analysis are now in progress).

The previous results, which allow to control the microstructure of the alloy and its influence on the magnetic behavior, are in full agreement with behaviors observed in similar alloy systems. Nevertheless, the possible spin glass behavior linked to the amorphous state (proposed in a similar Ni-Mn-In alloy [26]) and the evolution of

magnetism brought by the crystallization process needs to be analyzed in more detail. In this sense, magnetization and susceptibility measurements has been performed on the milled samples. Zero Field Cooled/Field Cooled/Field Heating (ZFC/FC/FH) curves at 100 Oe are shown in Figure 3. It can be seen that the longer the milling time the lower the magnetization of the amorphous phase. With respect to the temperature dependence of magnetization, the broad peak in the ZFC curve for the sample with lower milling time (10h) could be probably ascribed to a distribution of spin-glass states correlated to a certain inhomogeneity with different amorphization degree. The 40 hours as-milled sample, in turn, shows a spin glass behavior at low temperatures described by a sharp drop of the magnetization in the ZFC curve bellow 50 K [17] (see inset), pointing out a more homogenous amorphization. Focusing is this latter sample, the hysteresis loops measured at 5 K in both the as-milled state and after annealing at 453, 508 and 583 K (just above S, P1 and P2 peaks) are shown in Figure 4. A magnetic state with high coercivity (~2000 Oe), high magnetic anisotropy (non-saturated system) and low magnetization at 6T (8emu/g) characteristic of a frustrated system (spin glass) [16] is found for the as-milled sample. While no significant variation is observed on heating above S shoulder, a clear decrease in coercivity and a high increase in magnetization occurs on annealing at P1 and P2, above which a well-developed ferromagnetic state can be inferred. In particular, as shown in Figure 5, the high field magnetization (at $H=6T$) increases to 33 emu/g and 83 emu/g after 508 and 583 K, respectively in accordance with the proposed two-stage crystallization process. In fact, magnetic saturation occurs only after annealing at 583 K.

The spin-glass state of the amorphous structure has been analyzed in detail. Figure 6 shows the real part of the AC susceptibility at different frequencies within the 0.02-200 Hz range. It is well known that in the vicinity of the freezing temperature, spin glasses

exhibit an AC frequency dependence characterized by a shift in the observed maximum (ΔT_{max}) to higher temperatures when frequency ($\omega=2\pi f$) increases. The denominated c parameter defined as $\frac{\Delta T_{\max}}{T_{\max}\Delta \log_{10} \omega}$ is usually ascribed to the presence of the interaction strength between the nanoparticles. Regarding this fact, the difference between non interacting superparamagnetic systems (c>0.3), medium interaction regime (0.05<c<0.13) or interacting spin glasses (0.005<c<0.05) lies on the different value of c parameter, where a decrease of this value represents an increase of the magnetic interactions [13]. In this regard, the as-milled sample displayed a value of 0.02, within the limits established for interacting spin glasses systems. The magnitude of the real part of the susceptibility decreases with frequency since the magnetic moments cannot follow the magnetic field, in contrast to the expected increase in the imaginary part.

The frequency dependence of the freezing temperature is also well described by the Vogel Fulcher law in interacting systems, and defined by the following equation [16,27]:

$$f = f_0 \exp\left(\frac{E_a}{k_B(T_f - T_0)}\right)$$

where f is the frequency, f_0 a characteristic frequency, T_0 is a parameter that measures the interaction strength due to dipolar and exchange interaction between the clusters or magnetic moments, E_a is the activation energy and k_B the Boltzmann constant. The fitting to this exponential law (inset Fig. 6), led to T_0 = 47K, f_0 = 6.4 10^5 Hz and E_a/k_B = 40 K. Taking into account that T_0 = 0 is defined for systems with negligible magnetic interactions [19], the high value of T_0 indicates strong magnetic interactions between the magnetic moments. The coefficient $[T_f - T_0]/T_f$ (where T_f is the maximum temperature of the ZFC curve, and T_0 the temperature estimated from the fitting to Vogel Fulcher law)

is a parameter usually employed as an indication of a slow frequency dependence in canonical spin glasses (<0.1) or high dependence in cluster spin glasses (>0.5)[15,28]. Furthermore, the value of the characteristic frequency, $\tau_0 = 1/f_0$ for the different systems is also indicative of each type of spin glasses. Thus, τ_0 values above 10^{-4} s are related to canonical systems and bellow 10^{-7} s for cluster spin glasses [28]. In our case, the obtained parameters are $[T_f - T_0]/T_f = 0.04$ and $\tau = 10^{-5}$ s, so a canonical spin glass seems to be the most feasible explanation for the observed behavior.

In order to confirm the nature of the disordered system, Figure 7 shows the corresponding ZFC/FC curves measured at different applied magnetic fields (0.01 to 4 T). The shift of the maximum in the ZFC curves towards lower temperatures when the magnetic field increases can be attributed to a change in the energy barrier between the spin glass state and the high temperature magnetic state. Then, at a critical magnetic field the irreversibility in the ZFC/FC curves vanishes since the magnetic anisotropy of the frustrated state is overcome. Almeida and Thouless [29] described the line between the magnetic state at low temperatures and the corresponding state at high temperatures through the dependence of this energy barrier at different magnetic fields by means of the equation:

$$\left(H = H_0 \left(1 - \frac{T_p}{T_f} \right)^{3/2} \right)$$

where H_0 is the critical magnetic field, T_p the maximum temperature of the ZFC curves for the different magnetic fields and T_f the corresponding freezing temperature below which the spins are randomly oriented. In the inset of Figure 7 the correct fitting is represented with an estimated T_f value of 35K and a critical magnetic field of $\mu_0 H = 8$T,

indicating the existence of magnetic interactions comparing with the T_0 obtained from the Vogel Fulcher law fitting.

4. Conclusions

In short, increasing of the ball milling time in Ni-Mn-In alloys (longer than 40 h) induced the disappearance of the long-range atomic order and the subsequent occurrence of a frustrated magnetic system. A two-stage crystallization process to a cubic B2 structure takes place on annealing around 600 K, leading to a well-developed ferromagnetism. With respect to the amorphous stated, the AC frequency dependence of the ZFC/FC curves together with the parameters obtained from the Vogel Fulcher law and Almeida-Thouless approach applied to the freezing temperature indicates that a canonical spin glass could be the most feasible explanation for the observed behavior at low temperatures. This result is also in complete agreement with the evolution of the hysteresis loops observed at low temperatures.

Acknowledgements.-This work has been carried out with the financial support of the Spanish "Ministerio de Economía y Competitividad" and FEDER funding, project nº MAT2012-37923. I. Unzueta acknowledges financial support from Basque Government Grants nos. IT-443-10 and PRE_2014_214.

References

[1] R.Y. Umetsu, W. Ito, K. Ito, K. Koyama, A. Fujita, K. Oikawa, et al., Anomaly in entropy change between parent and martensite phases in the Ni50Mn34In16 Heusler alloy, Scr. Mater. 60 (2009) 25–28.

[2] I. Dubenko, T. Samanta, A. Kumar Pathak, A. Kazakov, V. Prudnikov, S. Stadler, et al., Magnetocaloric effect and multifunctional properties of Ni–Mn-based Heusler alloys, J. Magn. Magn. Mater. 324 (2012) 3530–3534.

[3] J. Pons, E. Cesari, C. Seguí, F. Masdeu, R. Santamarta, Ferromagnetic shape memory alloys: Alternatives to Ni–Mn–Ga, Mater. Sci. Eng. A. 481-482 (2008) 57–65.

[4] T. Miyamoto, W. Ito, R.Y. Umetsu, R. Kainuma, T. Kanomata, K. Ishida, Phase stability and magnetic properties of Ni50Mn50−xInx Heusler-type alloys, Scr. Mater. 62 (2010) 151–154.

[5] W. Ito, M. Nagasako, R.Y. Umetsu, R. Kainuma, T. Kanomata, K. Ishida, Atomic ordering and magnetic properties in the $Ni_{45}Co_5Mn_{36.7}In_{13.3}$ metamagnetic shape memory alloy, Appl. Phys. Lett. 93 (2008) 232503.

[6] E. Şaşıoğlu, L.M. Sandratskii, P. Bruno, First-principles calculation of the intersublattice exchange interactions and Curie temperatures of the full Heusler alloys Ni 2 Mn X (X = Ga , In , Sn , Sb), Phys. Rev. B. 70 (2004) 024427.

[7] E. Şaşıoğlu, L.M. Sandratskii, P. Bruno, Role of conduction electrons in mediating exchange interactions in Mn-based Heusler alloys, Phys. Rev. B. 77 (2008) 064417.

[8] K.R. Priolkar, D.N. Lobo, P. a. Bhobe, S. Emura, a. K. Nigam, Role of Ni-Mn hybridization in magnetism of martensitic state of Ni-Mn-In shape memory alloys, (2011) 1–10.

[9] L. Ma, W.H. Wang, J.B. Lu, J.Q. Li, C.M. Zhen, D.L. Hou, et al., Coexistence of reentrant-spin-glass and ferromagnetic martensitic phases in the Mn2Ni1.6Sn0.4 Heusler alloy, Appl. Phys. Lett. 99 (2011) 182507.

[10] V. Sánchez-Alarcos, J.I. Pérez-Landazábal, V. Recarte, I. Lucia, J. Vélez, J. a. Rodríguez-Velamazán, Effect of high-temperature quenching on the magnetostructural transformations and the long-range atomic order of Ni-Mn-Sn and Ni-Mn-Sb metamagnetic shape memory alloys, Acta Mater. 61 (2013) 4676–4682.

[11] V. Recarte, J.I. Pérez-Landazábal, V. Sánchez-Alarcos, Dependence of the relative stability between austenite and martensite phases on the atomic order in a Ni–Mn–In Metamagnetic Shape Memory Alloy, J. Alloys Compd. 536 (2012) S308–S311.

[12] V. Recarte, J.I. Pérez-Landazábal, V. Sánchez-Alarcos, J.A. Rodríguez-Velamazán, Dependence of the martensitic transformation and magnetic transition on the atomic order in Ni–Mn–In metamagnetic shape memory alloys, Acta Mater. 60 (2012) 1937–1945.

[13] B. Aslibeiki, P. Kameli, H. Salamati, M. Eshraghi, T. Tahmasebi, Superspin glass state in MnFe2O4 nanoparticles, J. Magn. Magn. Mater. 322 (2010) 2929–2934.

[14] S.N. Jammalamadaka, S.S. Rao, J. Vanacken, A. Stesmans, S. V. Bhat, V. V. Moshchalkov, Martensite-like transition and spin-glass behavior in nanocrystalline Pr0.5Ca0.5MnO3, AIP Adv. 1 (2011) 042151.

[15] S. Mukherjee, R. Ranganathan, P. Anilkumar, P. Joy, Static and dynamic response of cluster glass in $La_{0.5}Sr_{0.5}CoO_3$, Phys. Rev. B. 54 (1996) 9267–9274.

[16] A. Kumar, R.P. Tandon, V.P.S. Awana, Study of spin glass and cluster ferromagnetism in $RuSr_2$ $Eu_{1.4}$ $Ce_{0.6}$ Cu_2 O_{10} magneto Superconductor, 043926 (2011) 28.

[17] J.L. López, H.-D. Pfannes, R. Paniago, J.P. Sinnecker, M.A. Novak, Investigation of the static and dynamic magnetic properties of $CoFe_2O_4$ nanoparticles, J. Magn. Magn. Mater. 320 (2008) e327–e330.

[18] D. Aurongzeb, M. Holtz, L. Menon, Diffusion process and formation of super-spin-glass state in soft magnetic Fe/Pt system, Appl. Phys. Lett. 89 (2006) 092501.

[19] F.F. Barquín, J.C.G. Sal, P. Gorria, J.S. Garitaonandia, J.M. Barandiarán, Dynamic susceptibility of reentrant Fe-rich inhomogeneous amorphous alloys, Eur. Phys. J. B. 35 (2003) 3–12.

[20] S. Aksoy, Synthesis and characterization of NiMnIn nanoparticles, J. Magn. Magn. Mater. 373 (2015) 236–239.

[21] Y.D. Wang, Y. Ren, Z.H. Nie, D.M. Liu, L. Zuo, H. Choo, et al., Structural transition of ferromagnetic Ni_2MnGa nanoparticles, J. Appl. Phys. 101 (2007) 063530.

[22] B. Tian, F. Chen, Y. Liu, Y.F. Zheng, Structural transition and atomic ordering of Ni49.8Mn28.5Ga21.7 ferromagnetic shape memory alloy powders prepared by ball milling, Mater. Lett. 62 (2008) 2851–2854.

[23] R. Das, A. Perumal, A. Srinivasan, Effect of particle size on the magneto-caloric properties of Ni51Mn34In14Si1 alloy, J. Alloys Compd. 572 (2013) 192–198.

[24] K. Vallal Peruman, M. Mahendran, S. Seenithurai, R. Chokkalingam, R.K. Singh, V. Chandrasekaran, Internal stress dependent structural transition in ferromagnetic Ni–Mn–Ga nanoparticles prepared by ball milling, J. Phys. Chem. Solids. 71 (2010) 1540–1544.

[25] A. Ghotbi Varzaneh, P. Kameli, F. Karimzadeh, B. Aslibeiki, G. Varvaro, H. Salamati, Magnetocaloric effect in Ni47Mn40Sn13 alloy prepared by mechanical alloying, J. Alloys Compd. 598 (2014) 6–10.

[26] D.M. Liu, Z.H. Nie, Y. Ren, Y.D. Wang, J. Pearson, P.K. Liaw, et al., Structural Transitions and Magnetic Properties of Ni50Mn36.7In13.3 Particles with Amorphous-Like Phase, Metall. Mater. Trans. A. 42 (2011) 3062–3070.

[27] C.A. Cardoso, V.P.S. Awana, O.F. De Lima, H. Yamauchi, M. Karppinen, C. A. Cardoso, F. M. Araujo-Moreira V. P. S. Awana, E. Takayama-Muromachi, (2002).

[28] O.F. de Lima, J. a. H. Coaquira, R.L. de Almeida, S.K. Malik, Magnetic phase separation and cluster-spin-glass behavior in $LaMn_{1-x}Fe_xO_{3+y}$, J. Appl. Phys. 107 (2010) 09E107.

[29] J.R.L. de Almeida, D.J. Thouless, Stability of the Sherrington-Kirkpatrick solution of a spin glass model, J. Phys. A. Math. Gen. 11 (1978) 983–990.

Figure Captions

Figure 1. DSC themograms on the powder ball-milled samples. Inset: DSC thermogram for the parent bulk alloy.

Figure 2. XRD patterns for (a) the as-milled samples, and after heating up to (b) 536 K and (c) 673 K.

Figure 3. Zero Field Cooled / Field Cooled / Field Heating (ZFC/FC/FH) curves at 100Oe for the as-milled samples. Inset: ZFC/FC/FH for the sample with 40 h milling time.

Figure 4. Hysteresis loops at 5K in both the as-milled state and after annealing at 453, 508 and 583 K (40h sample).

Figure 5. Dependence of the M_{6T} at 5K in the amorphous state and after annealing treatments at 508 K and 583 K (40h sample). Line represents a guideline for the eye.

Figure 6. Temperature dependence of the real part of the susceptibility at different frequencies (0.2, 2, 20 and 200 Hz) (40h sample). Inset: Fitting to the Vogel Fulcher relation.

Figure 7. Zero Field Cooled / Field Cooled curves at different applied magnetic fields (0.01 - 4T) for the as-milled sample with 40 h. Inset: Fitting of the experimental data to the Almeida-Thouless law.

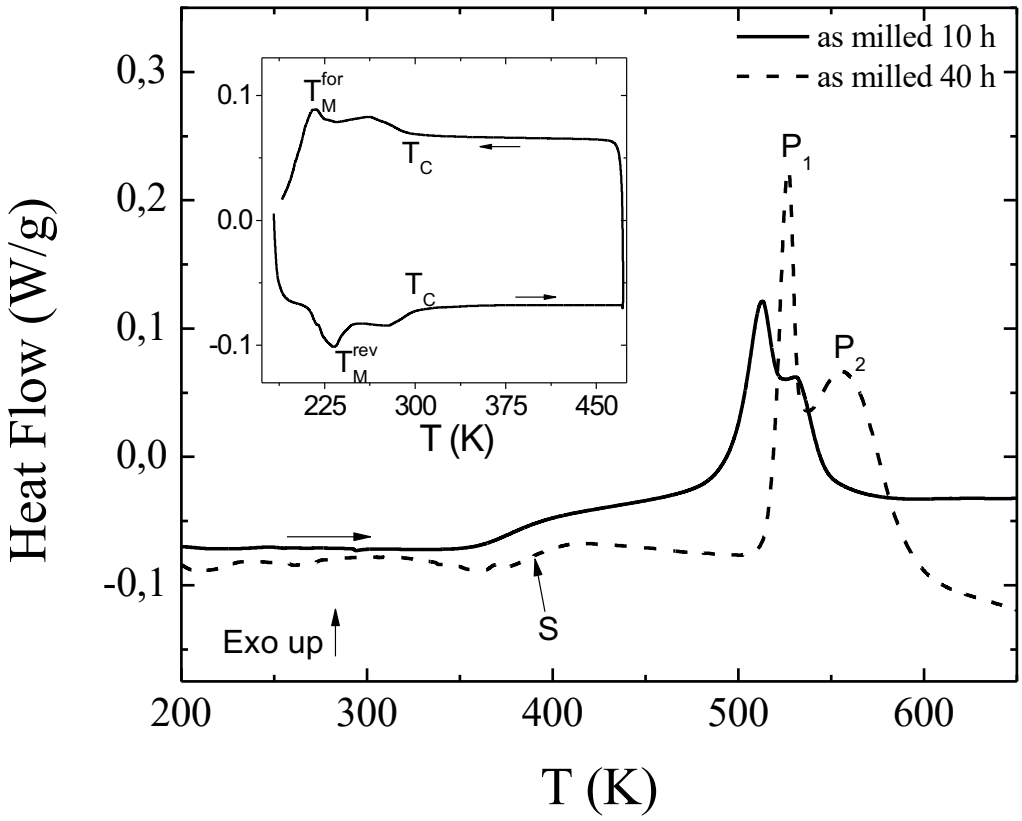
as milled 10 h
as milled 40 h
Heat Flow (W/g)
T (K)
P1
P2
S
Exo up
T_M^for
T_C
T_C
T_M^rev
T (K)

Figure 1

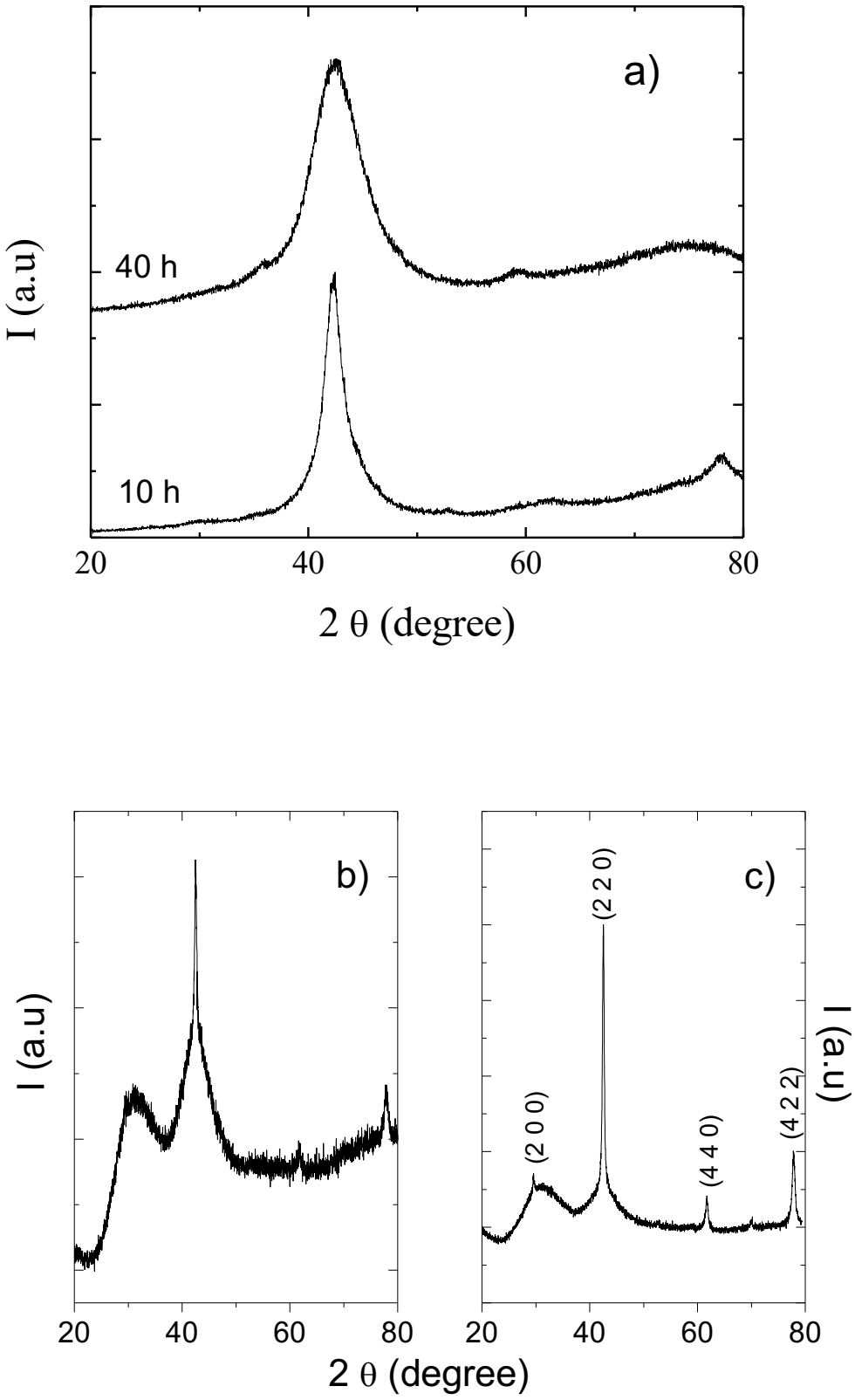
a)
40 h
10 h
I (a.u)
20
40
60
80
2 θ (degree)
b)
c)
(2 0 0)
(2 2 0)
(4 4 0)
(4 2 2)
I (a.u)
I (a.u)
20
40
60
80
20
40
60
80
2 θ (degree)

Figure 2

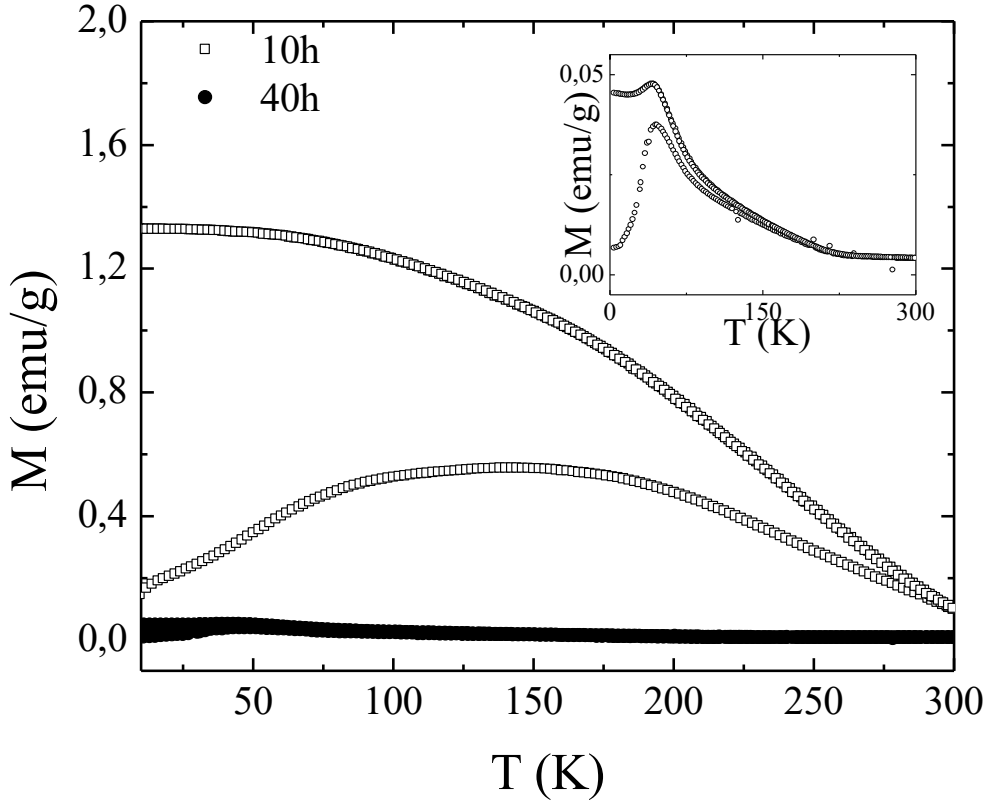
2,0
1,6
1,2
0,8
0,4
0,0
M (emu/g)
50
100
150
200
250
300
T (K)
10h
40h
0,05
0,00
M (emu/g)
0
150
300
T (K)

Figure 3

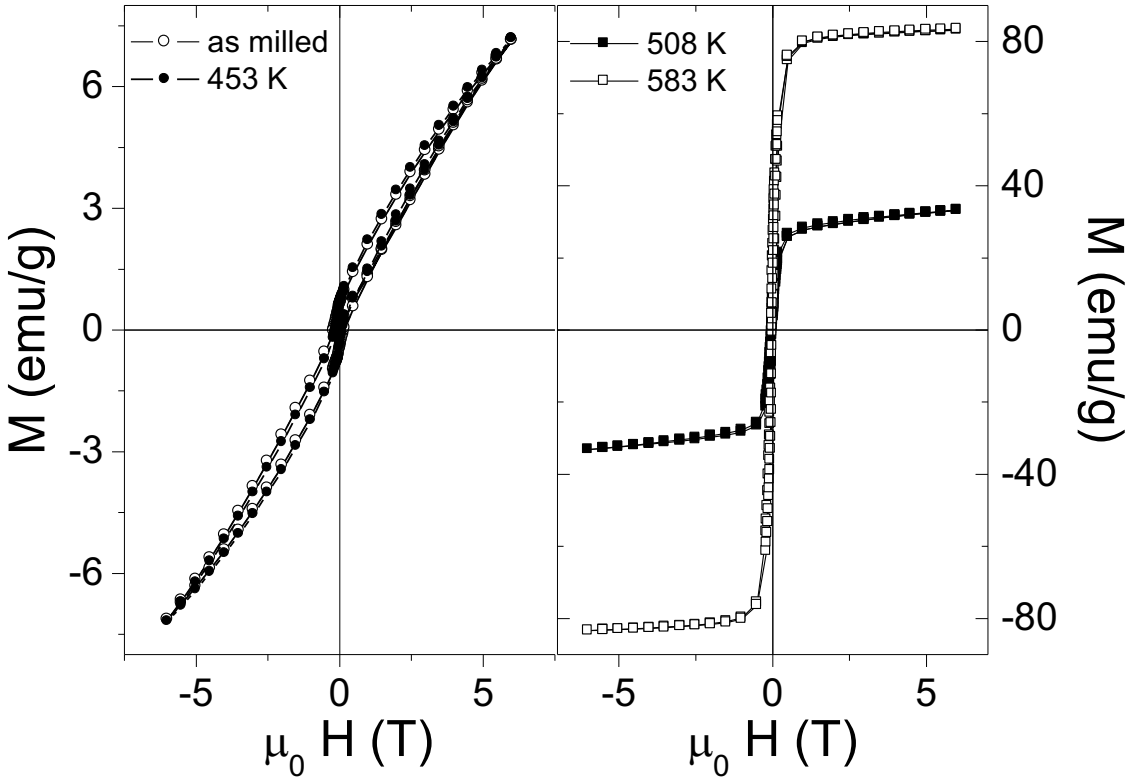
as milled
453 K
508 K
583 K
M (emu/g)
μ0 H (T)
μ0 H (T)
M (emu/g)
6
3
0
-3
-6
-5
0
5
-5
0
5
80
40
0
-40
-80

Figure 4

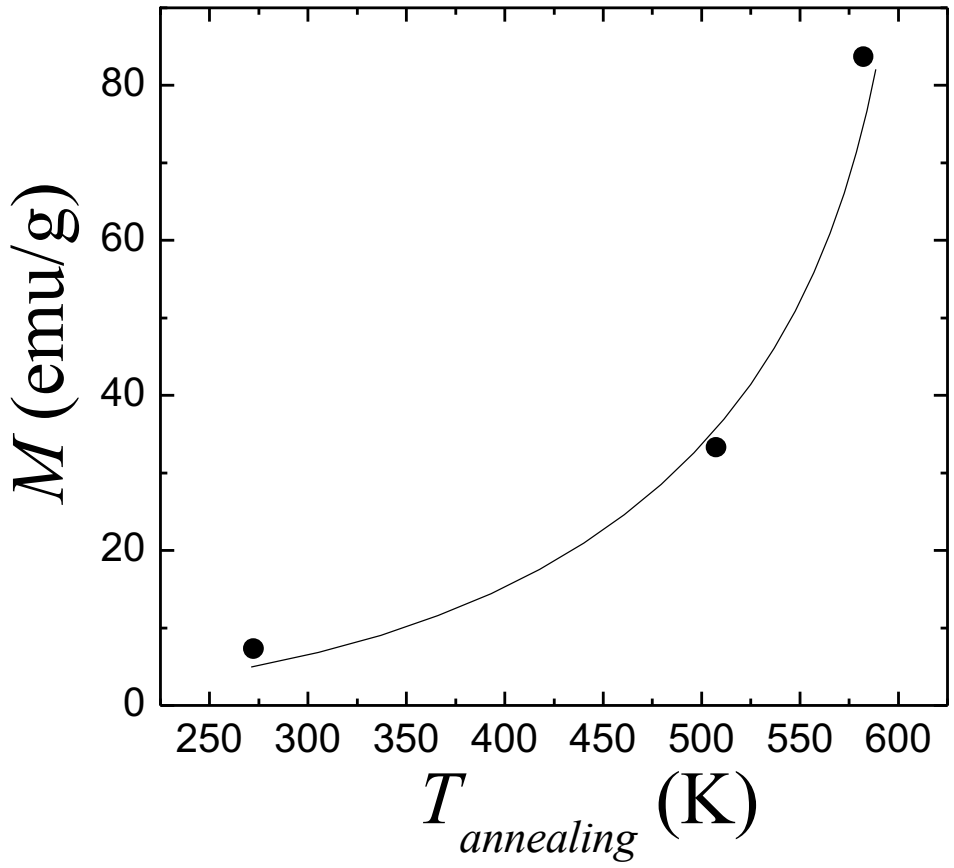

Figure 5

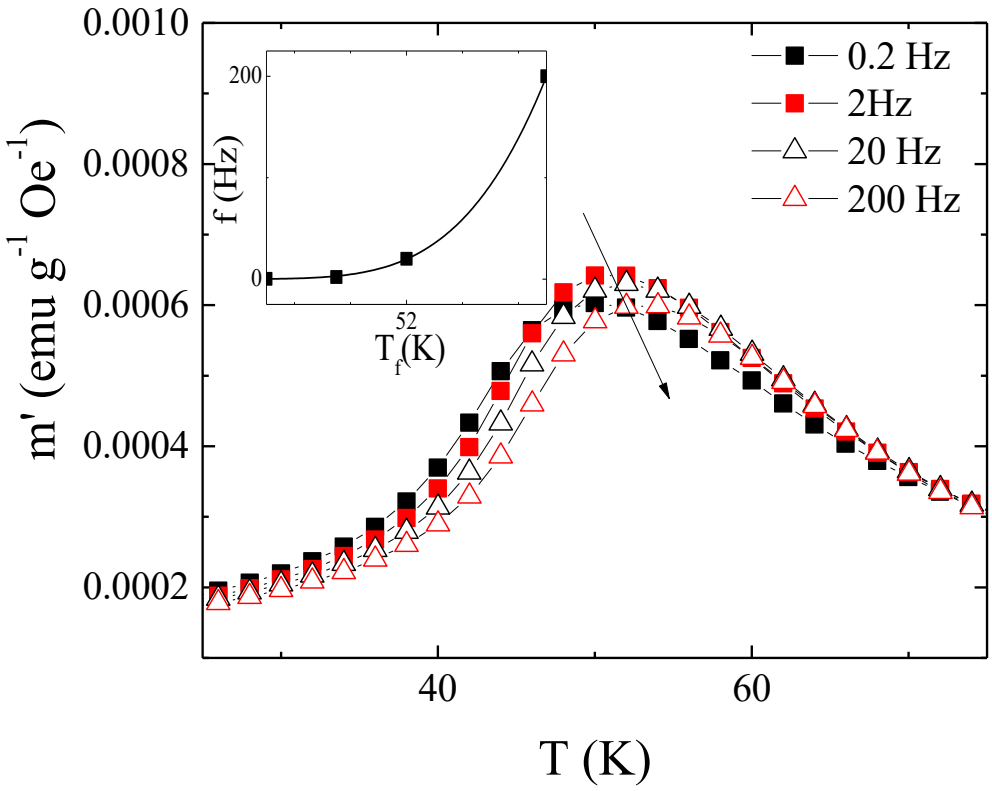
0.0010
0.0008
0.0006
0.0004
0.0002
m' (emu g-1 Oe-1)
40
60
T (K)
0.2 Hz
2Hz
20 Hz
200 Hz
200
0
f (Hz)
52
Tf(K)

Figure 6

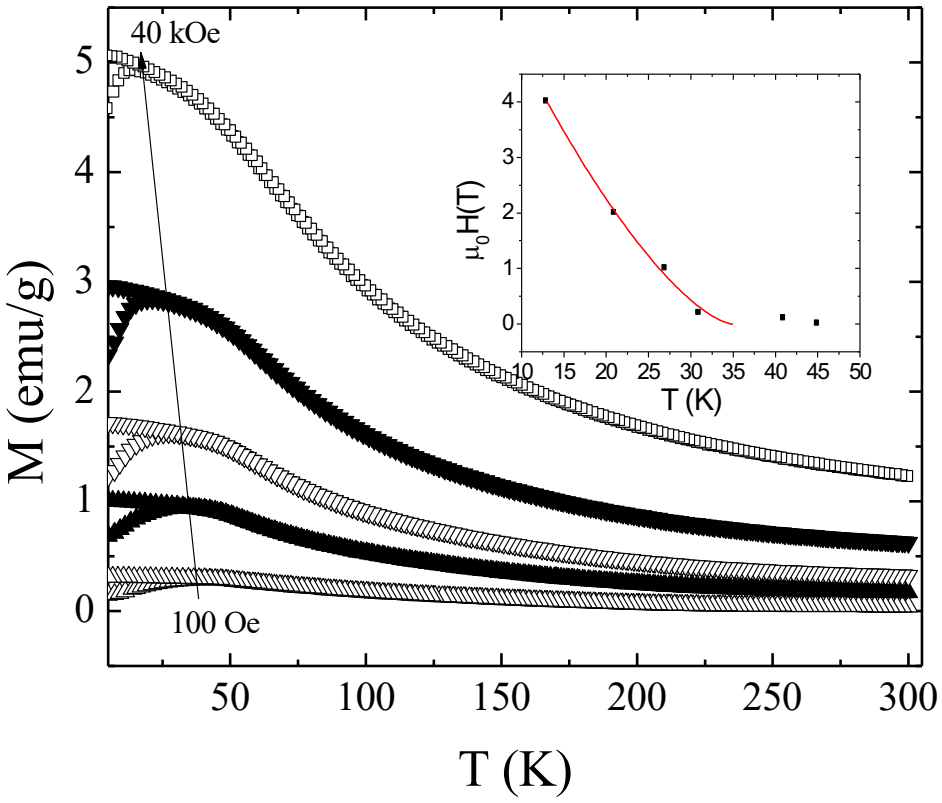

Figure 7